


Original Research

Inhibition of S100A9 Improves Aortic Dissection in Association With Mitochondrial Function Enhancement

Keyu Zhang^{1,2,3,†}, Linman Li^{4,†}, Yiying Zhang⁵, Kai Guo^{1,2}, Zhao Zhang^{1,2}, Mengning Wan⁶, Yongzheng Guo^{1,2}, Yu Zhao^{3,*}, Xiaowen Wang^{1,7,*} 

¹Cardiovascular Disease Laboratory, The First Affiliated Hospital of Chongqing Medical University, 400016 Chongqing, China

²Division of Cardiology, The First Affiliated Hospital of Chongqing Medical University, 400016 Chongqing, China

³Vascular Surgery Department, The First Affiliated Hospital of Chongqing Medical University, 400016 Chongqing, China

⁴Health Management Center, The First Affiliated Hospital of Chongqing Medical University, 400016 Chongqing, China

⁵Department of Epidemiology and Biostatistics, School of Public Health, Jiamusi University, 154000 Jiamusi, Heilongjiang, China

⁶Department of Anesthesiology, The First Affiliated Hospital of Chongqing Medical University, 400016 Chongqing, China

⁷Department of Thoracic and Cardiovascular Surgery, The First Affiliated Hospital of Chongqing Medical University, 400016 Chongqing, China

*Correspondence: 820994765@qq.com (Yu Zhao); xiaowenwang@cqmu.edu.cn (Xiaowen Wang)

†These authors contributed equally.

Academic Editor: Graham Pawelec

Submitted: 9 July 2025 Revised: 20 August 2025 Accepted: 29 August 2025 Published: 29 September 2025

Abstract

Background: Aortic dissection (AD) is a high-mortality cardiovascular emergency with unclear pathophysiological mechanisms. This study investigated S100 calcium-binding protein A9 (S100A9) as a therapeutic target for AD and explored its underlying mechanisms. **Methods:** Proteomic analysis compared aortic tissues from patients with acute type A and matched non-dissected vascular tissues from the same patients. An AD model was induced in wild-type and *S100A9* knockout mice via β -aminopropionitrile (BAPN). Survival, aortic diameter, and S100A9 expression were quantified. Furthermore, single-cell RNA sequencing was used to analyze cell populations and mitochondrial pathways in AD mice treated with an S100A9 inhibitor. Finally, the effect of S100A9 on mitochondrial function was investigated in Tohoku Hospital Pediatrics-1 (THP-1) cells. **Results:** Proteomics identified that S100A9 is significantly upregulated in AD tissue. Furthermore, *S100a9* knockout (*S100a9* KO) mice conferred protection against AD-induced mortality and aortic dilation. Single-cell RNA analysis revealed that S100A9 is predominantly expressed within the granulocyte population. *S100A9* inhibition activated mitochondrial oxidative phosphorylation pathways and upregulated mtDNA-encoded gene expression. Human tissue mRNA levels confirmed decreased mtDNA in AD. Moreover, recombinant human S100A9 and angiotensin-II treatment in THP-1 cells reduced mitochondrial membrane potential and increased oxidative stress. **Conclusions:** S100A9 is a potential contributor to AD pathogenesis. Inhibition of S100A9 might be a promising therapeutic target for AD.

Keywords: aortic dissection; proteomic analysis; single-cell RNA sequencing; mitochondrial function; S100A9

1. Introduction

Aortic dissection (AD) is a life-threatening cardiovascular disease characterized by high mortality rates and a poor prognosis [1]. AD initiation involves a tear in the aortic intima, causing separation of the aortic wall layers [2]. This process enables blood entry into the aortic media, ultimately resulting in organ ischemia, aortic rupture, and potentially sudden death [1]. Despite therapeutic advances, mortality remains high, primarily due to an incomplete understanding of AD's underlying pathogenic mechanisms.

The pathophysiology of aortic dissection involves inflammation and oxidative stress. Granulocyte macrophage colony-stimulating factor (GM-CSF), a pro-inflammatory cytokine, contributes critically to AD development [3,4]. Furthermore, interleukin-6 (IL-6) serves as an essential mediator of angiotensin-II (Ang-II)-induced aortic dissection [5]. Notably, experimental evidence from mouse models demonstrates that increased reactive oxygen species (ROS)

levels are associated with aortic dissection [6]. Consequently, targeting inflammatory responses and ROS generation may represent promising therapeutic strategies for AD [7]. Despite this potential, the specific cytokines mediating inflammation and oxidative stress in AD pathogenesis remain poorly characterized.

S100A9, a member of the S100 protein family, functions as a small calcium-binding protein primarily involved in inflammatory processes and immune responses [8]. It is frequently upregulated in response to diverse inflammatory stimuli and has been implicated in various cardiovascular pathologies, including myocardial infarction, heart failure, and age-induced vascular dysfunction [9]. Our prior work has associated elevated S100A9 levels with sepsis-induced acute respiratory injury [10]. Emerging evidence suggests that pharmacological S100A9 inhibition may protect against aortic dissection pathophysiology by mitigating inflammatory responses [11]. However, the precise mechanisms remain incompletely understood.



This study aims to identify novel molecular targets indicative of aortic dissection progression and investigate their functional roles and mechanisms. Leveraging proteomic analysis of human patients with type A aortic dissection tissues, we identified that S100A9 was significantly upregulated in AD. Functioning as an S100 protein family member, S100A9 mediates diverse cellular processes such as inflammation and immune responses [12]. Our findings demonstrate that S100A9 inhibition improves survival in experimental AD mouse models and ameliorates AD-related outcomes, potentially through enhanced mitochondrial function and mitochondrial DNA expression. Collectively, these findings position S100A9 as a potential contributor to AD pathogenesis, establishing its inhibition as a possible therapeutic strategy.

2. Materials and Methods

2.1 Human Aorta Specimen Collection and Proteomic Sequencing

Human aortic dissection specimens and non-dissected vascular tissues (harvested distant from the dissection site) were obtained from patients undergoing surgery for type A aortic dissection. Samples were collected during aortic root and ascending aorta replacement surgeries at either the Department of Thoracic and Cardiovascular Surgery of Chongqing University Central Hospital and the First Affiliated Hospital of Chongqing Medical University from April 2024 to June 2024. All procedures received prior approval from the hospital's ethics committee and for this retrospective analysis of anonymized clinical data, the requirement for written informed consent was waived by the Ethics Committee (2024-173-02) and all procedures conducted in accordance with the Declaration of Helsinki. Protein was extracted from aortic tissue samples and digested with trypsin. The resulting peptides underwent liquid chromatography-tandem mass spectrometry (LC-MS/MS) analysis using high-resolution mass spectrometer. The acquired spectra were processed using a database to identify and quantify the proteins. Label-free quantification (LFQ) was used to analyze differential protein expression between dissection and control tissues.

2.2 Experimental Animals and Aortic Dissection Model

Male C57BL/6J mice and global *S100a9* knockout (KO) mice were purchased from Cyagen Biosciences Inc (Suzhou, China) and housed under specific pathogen-free conditions at the Chongqing Medical University Animal Research Center. Aortic dissection was induced in both wild-type (WT) and *S100a9* KO mice. Starting from week 6, all mice were received daily β -aminopropionitrile (BAPN, Cat: A3134-5G, Sigma, Milano, Italy) dissolved in drinking water at a dose of 1 g/kg/day. During the aortic diameter examination, mice were anesthetized and maintained with isoflurane (3% for induction, followed by 1.5% for maintenance), and aortic diameter was assessed using

VINNO 6 VET ultrasound system for small animals. For euthanasia, intravenous thiopental sodium (150 mg/kg) was administered. The drug was prepared at a concentration of 25 mg/mL in sterile saline and injected via the tail vein. Then thoracic aortas were harvested, snap-frozen in liquid nitrogen, and stored at -80°C for subsequent analysis. All animal procedures were approved by the Animal Care and Use Committee of Chongqing Medical University (IACUC-CQMU-2024-04098).

2.3 Western Blot

Protein lysates were resolved by SDS-PAGE (Cat: PG212, EpiZyme, Shanghai, China) at 80–120 V constant voltage. Separated proteins were electrophoretically transferred onto PVDF membranes (Cat: ISEQ00010, Millipore, Billerica, MA, USA) using a rapid transfer solution at 400 mA for 30 minutes. The membranes were blocked with 5% skim milk (Cat: D8340, Solarbio, Beijing, China) for 1.5 hours and washed three times with TBST (Cat: G0001-2L, Servicebio, Wuhan, Hubei, China) for 3 minutes each. Primary antibodies S100A9 (1:1000, Cat: ab288715, Abcam, Cambridge, UK), GAPDH (1:10,000, Cat: GB11002, Servicebio, Wuhan, Hubei, China) were incubated overnight at 4°C , followed by incubation with secondary antibodies (1:7000, Cat: AB-228395, Invitrogen, Carlsbad, CA, USA) the next day. The signal was visualized by enhanced chemiluminescence (Cat: BL520B, Biosharp, Beijing, China).

2.4 The RT-qPCR Analysis

Total RNA was extracted from tissue samples using Trizol (Takara, Beijing, China). The RNA was then reverse-transcribed into cDNA using a reverse transcription kit (Cat: RK20433, ABclonal, Wuhan, Hubei, China). Quantitative PCR was performed using SYBR Green Master Mix with specific primers (Cat: RK21203, ABclonal, Wuhan, Hubei, China) on a CFX96™ Real-Time system (Bio-Rad Laboratories, Inc., Hercules, CA, USA). The mRNA expression levels were normalized to β -ACTIN using the delta-delta Ct ($2^{-\Delta\Delta\text{Ct}}$) relative quantification method. The PCR primer sequences used for measuring mRNA expression are presented below (F, R): β -ACTIN human: (CCTTCCTGGGCATG-GAGTC, TGATCTTCATTGTGCTGGGTG); S100A9 human: (ATACTCTAGGAAGGAAGGACACC, TC-CATGATGTCATTTATGAGGGC); MT-CO1 human: (CCTACTCCTGCTCGCATCTG, AGAGGGGCGTTTGTATTGG); MT-ND1 human: (CGATTCCGCTACGAC-CAACT, AGGTTTGAGGGGGAATGCTG); MT-ND2 human: (ACCATCTTTGCAGGCACACT, GCTTCTGTGGAACGAGGGT); MT-ND3 human: (GCGGCTTC-GACCCTATATCC, AGGGCTCATGGTAGGGGTAA); MT-ND4 human: (GCTCCATCTGCCTACGACAA, GCTTCAGGGGGTTTGATGA); MT-ND5 human: (CGGAAGCCTATTCGAGGAT, ATAGGGGATTGTGCGGTGTG); MT-CYB human: (CCACCCCATC-

CAACATCTCC, GCGTCTGGTGAGTAGTGCAT);
MT-ATP8 human: (CCTACCTCCCTCACCAAAGC,
AGGATTGTGGGGGCAATGAAT).

2.5 Multi-Omics Data Analysis

2.5.1 Gene Ontology (GO) Enrichment Analysis and Gene Set Enrichment Analysis (GSEA) Analysis

GO enrichment analysis and visualization were performed using the ClusterProfiler (v4.10.1) in R studio (v4.3.2) [13]. GSEA enrichment analysis was conducted using the GSEABase (v1.64.0, Bioconductor Core Team, Seattle, WA, USA) [14]. All visualization results presented in the main text had Benjamini-Hochberg adjustment for multiple comparisons ($p_{\text{adj}} < 0.05$).

2.5.2 Protein-Protein Interaction Networks (PPI)

We constructed a PPI network by STRING (Search Tool for the Retrieval of Interacting Genes/proteins; v12.0, <https://string-db.org>). We then visualized PPI and identified hub genes within this network using the Cytoscape (v3.10.2, University of California, San Diego (UCSD), San Diego, CA, USA) and the MCODE plugin (v2.0.3).

2.5.3 GOSemSim Analysis

GOSemSim analysis was conducted in R studio using the GOSemSim package (v2.28.1) to comprehensively score candidate proteins from the aspects of Biological process, Molecular Function, and Cellular Component [15]. The analysis results were visualized using ggplot2 (v3.5.2), results had Benjamini-Hochberg adjustment for multiple comparisons ($p_{\text{adj}} < 0.05$).

2.5.4 Single-Cell RNA Sequencing Analysis

GSE247260 raw data was downloaded from GEO database. Single cells were extracted under the criteria: nFeature_RNA >300, nFeature_RNA <6000, nCount_RNA <20,000, percent.mt <10. Normalization, scaling, and clustering of cells were performed using the Seurat (v5.0.3, Satellite Biosciences, NY, USA) [16], which identified main cell types. The results were visualized using Uniform Manifold Approximation and Projection (UMAP).

2.6 Cell Culture

The human acute monocytic cell line Tohoku Hospital Pediatrics-1 (THP-1) was purchased from the Procell system (CL-0233, Wuhan, China), authenticated by STR profiling with no evidence of cross-contamination and tested negative for mycoplasma contamination. The cells were cultured in Complete Medium For Cell Culture Tested (Cat: TCH-G361-C, HyCyte, Suzhou, China) and supplemented with 10% fetal Bovine serum (FBS) (Cat: FBP-S005, HyCyte, Suzhou, China) in a humidified atmosphere at 37 °C under 5% CO₂. A working cell bank was produced from one of the master cell banks and the cells in the second or

third passage were used for experiments. The cells were diluted to 2×10^5 cells/mL three times a week and were in the exponential growth phase for all experiments.

2.7 Statistical Analysis

Data were analyzed using GraphPad Prism software (v8.0.2, GraphPad Software, LLC, San Diego, CA, USA). Results are presented as mean \pm standard deviation (SD). Statistical comparisons between groups were made using one-way Analysis of Variance (ANOVA), with a p value < 0.05 considered statistically significant.

3. Results

3.1 Proteomics Analysis Revealed S100A9 as a Potential Hub Protein in Aortic Dissection

Paired aortic tissue specimens (five dissected and five matched non-dissected vascular samples) were obtained from patients undergoing surgical repair for acute Type A aortic dissection. All ten samples underwent proteomic profiling via LC-MS/MS. Following stringent quality control, 4608 proteins were confidently identified. Principal component analysis (PCA) validated dataset integrity, showing a significant separation between dissection and control groups (Fig. 1A). Differential expression analysis identified 190 significantly altered proteins ($|\log_2\text{FC}| > 1.2$, $p_{\text{adj}} < 0.05$), with 120 proteins upregulated and 70 downregulated proteins relative to controls (Fig. 1B,C). GO enrichment analysis revealed significant enrichment ($p_{\text{adj}} < 0.05$) of differentially expressed proteins in biological processes related to the response to lipopolysaccharides, molecular functions such as glycosaminoglycan and Toll-like receptor binding, and cellular components associated with secretory granules (Fig. 1D–F, **Supplementary Table 1**). Further GSEA further confirmed significant activation (Nonparametric Estimation Statistics (NES) >1.8, $p_{\text{adj}} < 0.05$) of inflammatory and lipopolysaccharide responses (Fig. 1G,H, **Supplementary Table 2**).

To characterize functional interactions among differentially expressed proteins, we conducted a PPI network using the STRING database (v12.0). Among the 190 input proteins, 52 lacked predicted interactions, while five formed disconnected singleton pairs (Fig. 2A, **Supplementary Table 3**). After filtering out these non-networked proteins, the remaining 133 proteins were ranked by topological importance in Cytoscape (v3.10.2), with the highest-scoring hubs visualized at the network core (Fig. 2B, **Supplementary Table 4**). Topological analysis revealed high-scoring hub proteins concentrated at the network core, indicating functional centrality. Subsequent MCODE clustering identified 17 potential hub proteins from densely interconnected modules (Fig. 2C, **Supplementary Table 5**). To pinpoint the most significant hub protein, we calculated semantic similarity (GOSemSim v3.8, Bioconductor Core Team, Guangzhou, Guangdong, China) across three GO domains: biological process, molecular functions, and cellular

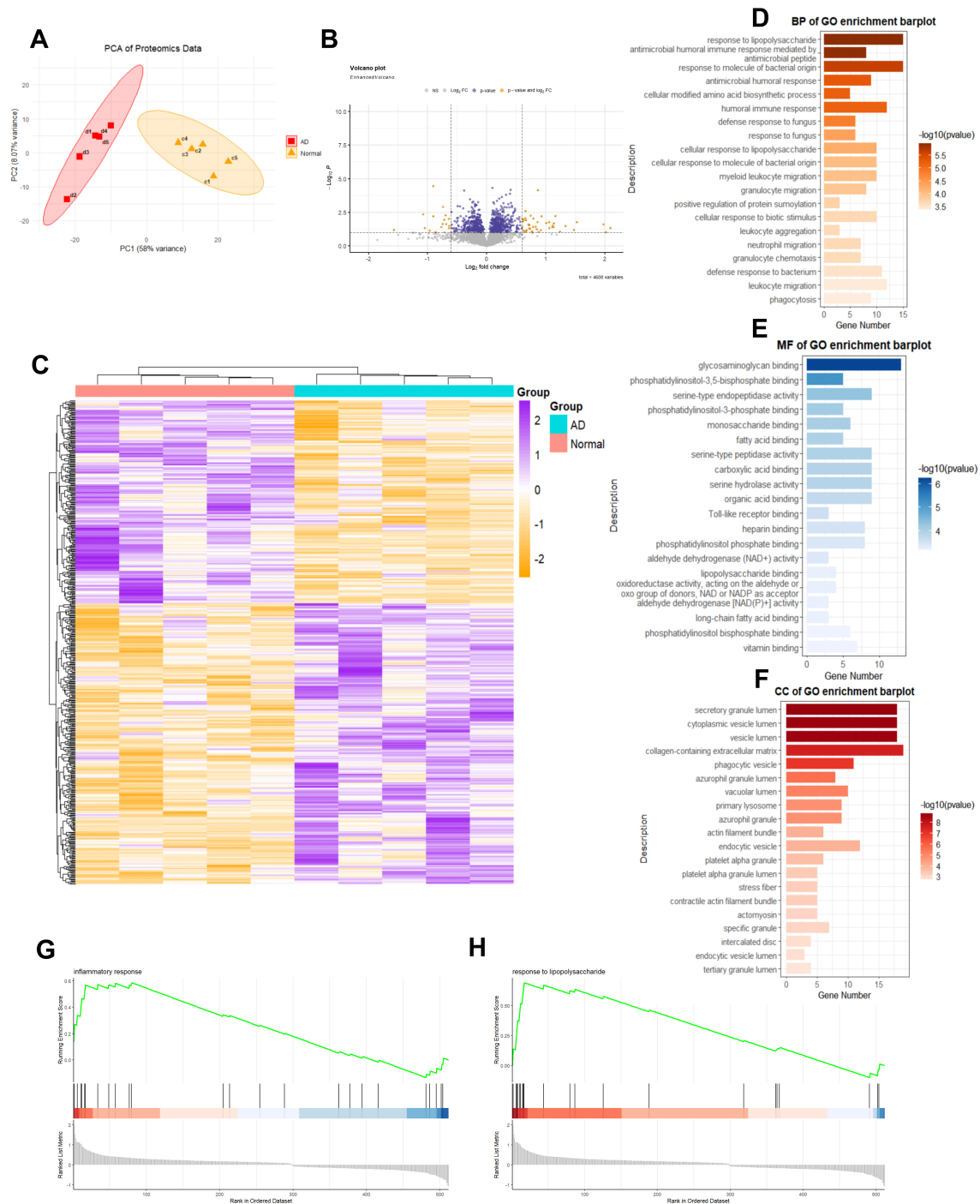


Fig. 1. Proteomic sequencing and analysis of type A aortic dissection (n = 5 for normal and dissection vascular samples). (A) Principal Component Analysis (PCA) of the proteomic data. (B) Volcano plot illustrating variable proteins (total proteins analyzed = 4608). (C) Heatmap depicting identified differential proteins. (D–F) Gene Ontology (GO) enrichment analysis of the differential proteins identified in proteomics ($p_{\text{adj}} < 0.05$). (G,H) Gene Set Enrichment Analysis (GSEA) for the differential proteins ($\text{NES} > 1.8$, $p_{\text{adj}} < 0.05$). NES, Nonparametric Estimation Statistics.

components. S100A9 demonstrated the highest functional coherence score (Fig. 2D). Correlation heatmap analysis showed that S100A9 was closely associated with S100A8 and exhibited interactions with other genes (Fig. 2E). Visualization through heatmap and volcano plot confirmed

significant upregulation of S100A9 in the aortic dissection group (Fig. 2F,G). These findings position S100A9 as a central regulator in aortic dissection.

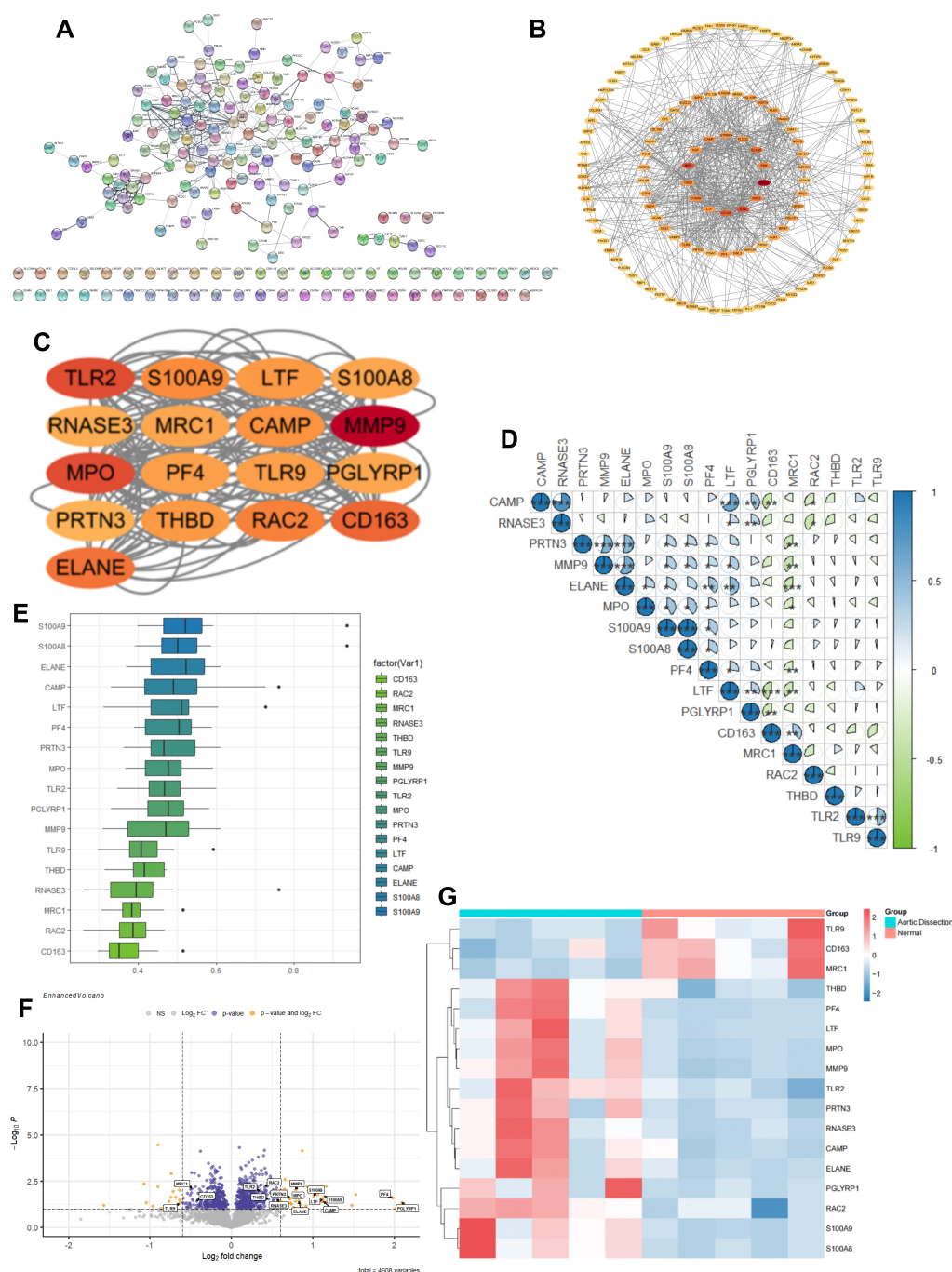


Fig. 2. Hub protein screening for type A aortic dissection. (A) Interaction network of differential proteins analyzed using the Search Tool for the Retrieval of Interacting Genes/proteins (STRING) database. (B) Importing protein interaction results into Cytoscape and ranking the proteins. (C) Identification of 17 hub proteins from the analysis of 138 proteins using the MCODE plugin. (D,E) Box plot and correlation heatmap of the final ranking for the 17 hub proteins from GOSensim analysis. (F) Volcano plot of the 17 hub proteins. (G) Heatmap of the 17 hub proteins, displaying each group separately. * $p < 0.05$; ** $p < 0.01$; *** $p < 0.001$.

3.2 *S100a9* Knockout Alleviates Aortic Dissection in Mouse Model

Following the identification of *S100A9* as a hub protein, we validated its expression in dissection vessels. Tissue proteins were extracted from both aortic dissection samples and normal vascular tissues. Western blot analysis

revealed a significant increase in *S100A9* expression in the aortic dissection group, consistent with proteomic data (Fig. 3A,B). Quantitative PCR further confirmed a marked upregulation of *S100a9* mRNA levels (Fig. 3C).

To explore the effects of *S100A9* on aortic dissection development, we utilized wild-type mice and *S100a9*

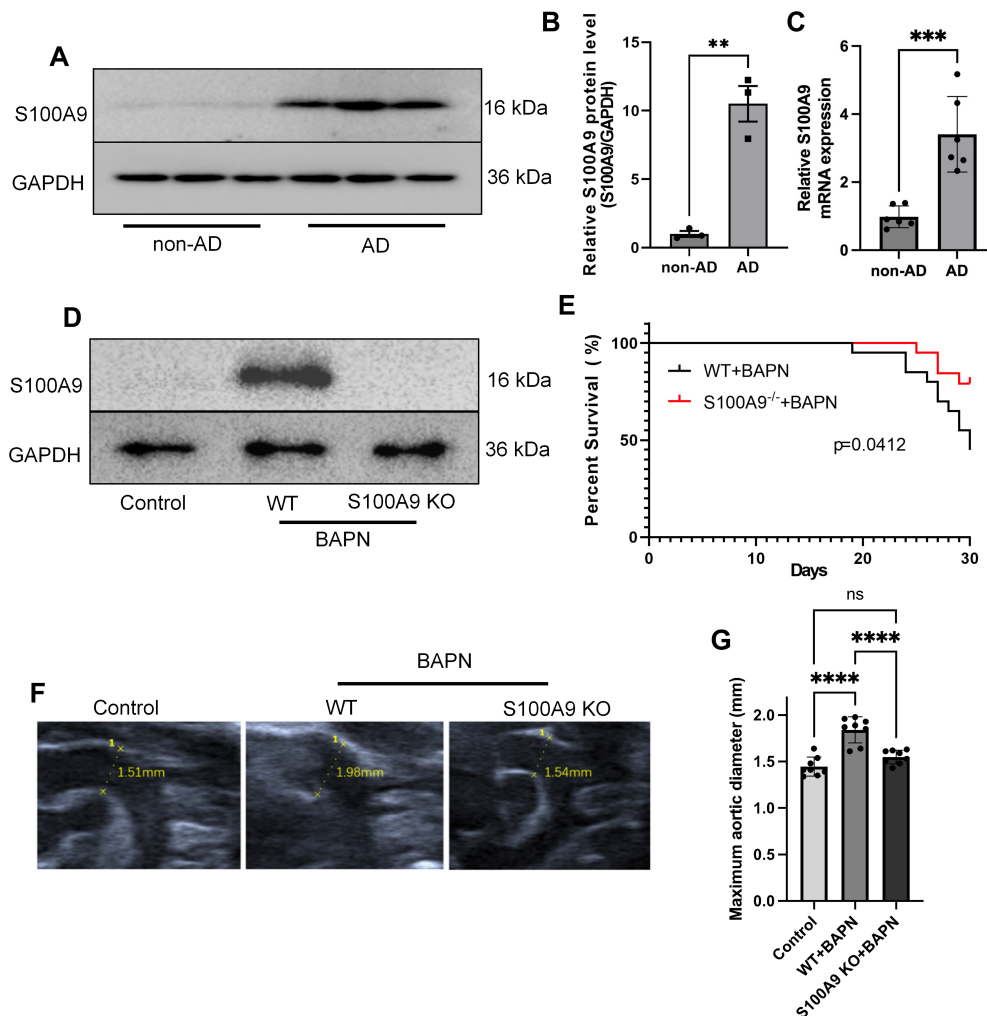


Fig. 3. Role of S100A9 in aortic dissection animal models. (A,B) Protein expression of S100A9 in aortic tissues from AD patients evaluated through Western blotting, with statistical analysis presented in (B) ($n = 3$). (C) *S100a9* mRNA expression in vascular tissues ($n = 6$). (D) Protein expression of S100A9 in aortic tissues evaluated through Western blotting ($n = 3$). (E) Survival analysis of WT and *S100a9* KO AD mice (45% vs 80%; p value = 0.0412). (F,G) Aortic diameter of mice across groups and the statistical result (p value < 0.0001). The data are presented as the mean \pm standard error of the mean. ns, no significant difference; ** $p < 0.01$; *** $p < 0.001$; **** $p < 0.0001$.

KO mice to induce aortic dissection model. Western blot analysis revealed that S100A9 levels were significantly elevated in the aortic vessels of BAPN-treated WT mice, while expression was nearly undetectable in *S100a9* KO mice treated with BAPN (Fig. 3D). *S100a9* KO significantly increased survival rates of AD mice (Hazard ratio *S100a9*^{-/-}+BAPN/WT+BAPN: 0.3236; 95% CI of ratio: 0.1143–0.9155, p value = 0.0412; Fig. 3E). Doppler ultrasound examinations showed that *S100a9* deficiency also decreased the aortic diameter in AD mice (p value < 0.0001; Fig. 3F,G). These findings indicate that S100A9 elevation drives AD pathogenesis in mice, while its inhibition markedly improves the condition, suggesting it could be a potential therapeutic intervention for aortic dissection.

3.3 Single-Cell Analysis Reveals Distinct Cell Populations upon *S100A9* Inhibition

To further investigate the mechanisms by which S100A9 influences aortic dissection, we analyzed single-cell sequencing data of aortic tissues from both aortic dissection models and ABR (paquinimod)-treated dissection models (ABR, an S100A9-specific inhibitor, intragastric administration, 10 mg/kg/d, single-cell dataset GEO247260) [11]. Using the Seurat package, we performed rigorous quality control, dimensionality reduction, and unsupervised clustering, identifying 15 distinct clusters (Fig. 4A). Through manual cell type annotation based on literature and marker databases (Fig. 4B,C). The results indicated that the proportions of B cells, T cells, Granulocyte, Macrophage, and Endothelial cells were significantly elevated in the dissection group compared to the treated group,

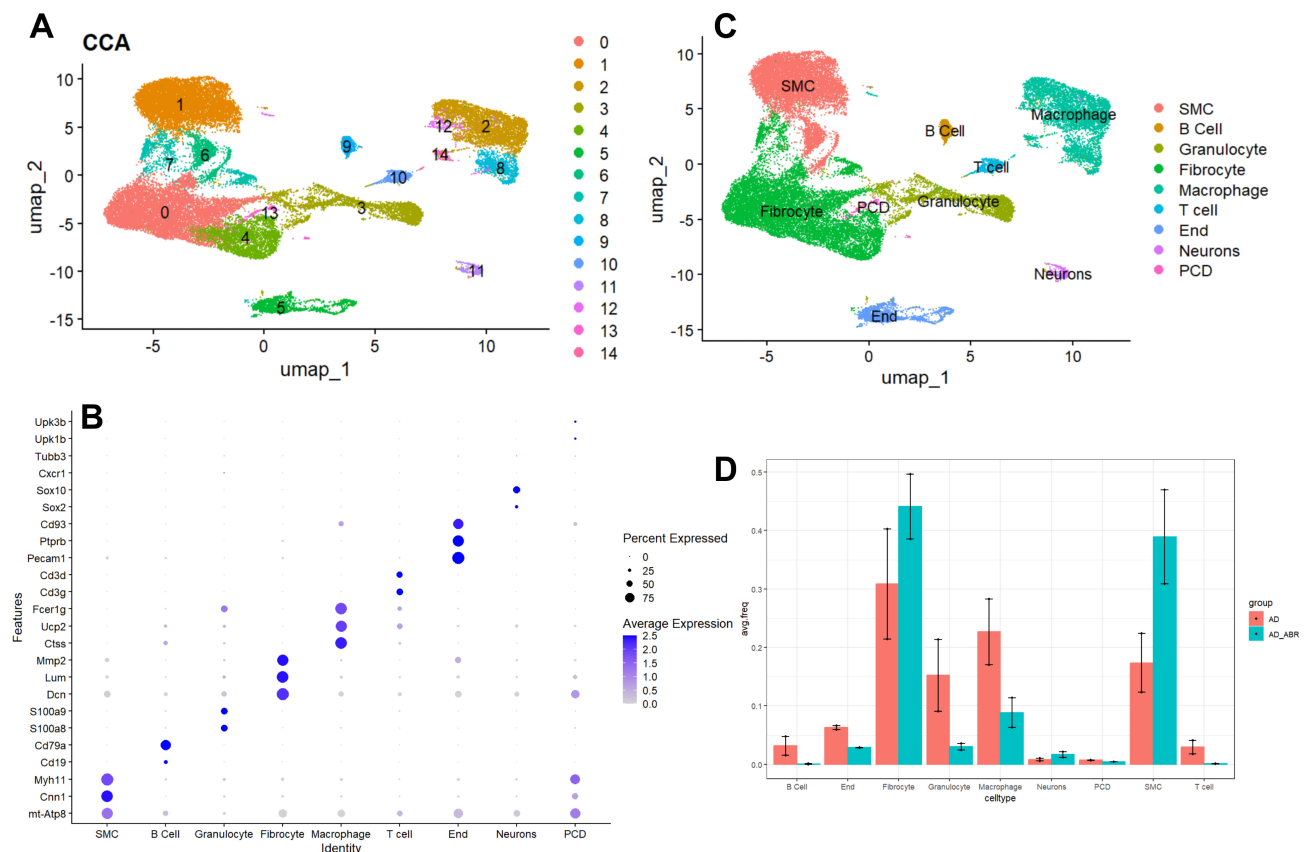


Fig. 4. Single-cell transcriptomic analysis of aortic dissection animal models with S100A9 intervention. (A) UMAP plot showing dimensionality reduction and clustering analysis of the GSE247260 dataset. (B) Bubble plot displaying the markers for each cluster. (C) UMAP plot illustrating the clustering based on marker expression. (D) Bar graph comparing the cell populations between the AD and AD+ABR groups (ABR, S100A9 inhibitor; 10 mg/kg/d).

while Fibrocyte and Smooth muscle cells (SMC) were more prevalent in the treated group (Fig. 4D). This suggests that inhibiting S100A9 expression leads to an increase in cell populations involved in vascular structure while reducing the numbers of immune and inflammatory cells. These findings align with our observation that deletion of *S100a9* improved the aortic dissection phenotype in BAPN-treated mice.

3.4 Inhibition of S100a9 Mitochondrial Quality in Granulocyte

Our analysis confirmed that *S100a9* is predominantly expressed in granulocyte (Fig. 5A). To elucidate the mechanisms involved, we performed single-cell Gene Set Variation Analysis (GSVA; v1.50.2, <https://bioconductor.org/packages/GSVA/>) specifically on granulocyte. We found that the oxidative phosphorylation pathway was significantly downregulated in granulocyte from the aortic dissection group compared to the treated group, indicating that inhibiting S100A9 expression enhances mitochondrial function (Fig. 5B). GO enrichment analysis for the granulocyte population revealed significant enrichment of the reactive oxygen species (ROS) pathway in the dissection group ($p_{\text{adj}} <$

0.05; Fig. 5C). Further examination of core mitochondrial genes demonstrated S100A9 inhibition (Fig. 5D,E) significantly increases in the expression levels of *mt-Nd1*, *mt-Nd2*, *mt-Nd3*, *mt-Nd4*, *mt-Nd5*, *mt-Cytb*, *mt-Co1*, and *mt-Atp8* following (Fig. 5F–M). These results suggest that enhanced mitochondrial quality may be responsible for the protective effects of *S100A9* knockout.

3.5 S100A9 Promotes Mitochondrial Dysfunction and Oxidative Stress In Vitro

To validate the single-cell analysis, we measured mRNA levels of key mitochondrial genes. *MT-CO1*, *MT-ND1*, *MT-ND2*, *MT-ND3*, *MT-ND4*, *MT-ND5*, *MT-CYB*, and *MT-ATP8* were significantly downregulated in human AD tissues (Fig. 6A–H). Using THP-1 cells, we further assessed the role of S100A9 in mitochondrial function. JC-1 staining showed reduced mitochondrial membrane potential, and MitoSOX staining revealed increased oxidative stress after treatment with Ang-II (Fig. 6I) and recombinant human S100A9 (rhS100A9) (Fig. 6J). These findings indicate that S100A9 deteriorate mitochondrial quality, targeting S100A9 to improve mitochondrial quality may offer a therapeutic strategy for aortic dissection.

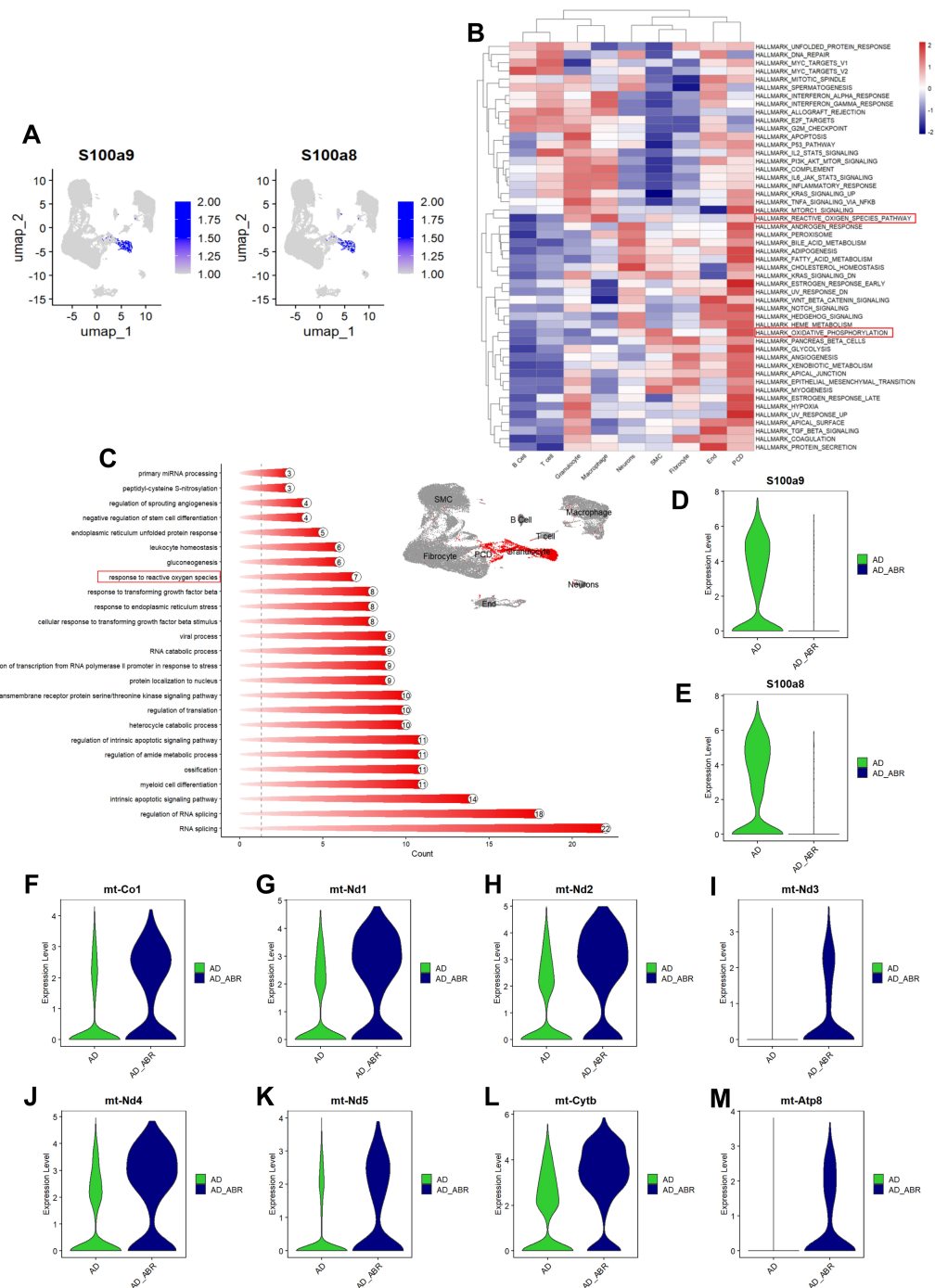


Fig. 5. Inhibition of S100a9 mitochondrial quality in granulocytes. (A) UMAP plots displaying the separate visualization of S100A9 and S100A8. (B) GSVA on granulocyte, with the visualized heatmap was reflecting changes in AD group ($p_{adj} < 0.05$). Related pathways marked by red boxes mean that the oxidative phosphorylation pathway was significantly downregulated in granulocytes from the aortic dissection group compared to the treated group. (C) Bar graph showing GO enrichment analysis for the granulocyte population ($p_{adj} < 0.05$). The related pathway marked by a red box means that GO enrichment analysis for the granulocyte population revealed significant enrichment of the reactive oxygen species (ROS) pathway in the dissection group. (D–M) Violin plots illustrating the differential expression of key mitochondrial genes in granulocyte population after S100A9 inhibition ($p_{adj} < 0.0001$).

4. Discussions

Aortic dissection is a complex and life-threatening condition characterized by the separation of the layers of the

aortic wall [5]. Our study highlights the role of S100A9 as a central player in the pathology of aortic dissection. Our proteomic analysis identified S100A9 as a hub protein, demonstrating its significant upregulation in aortic tissue from pa-

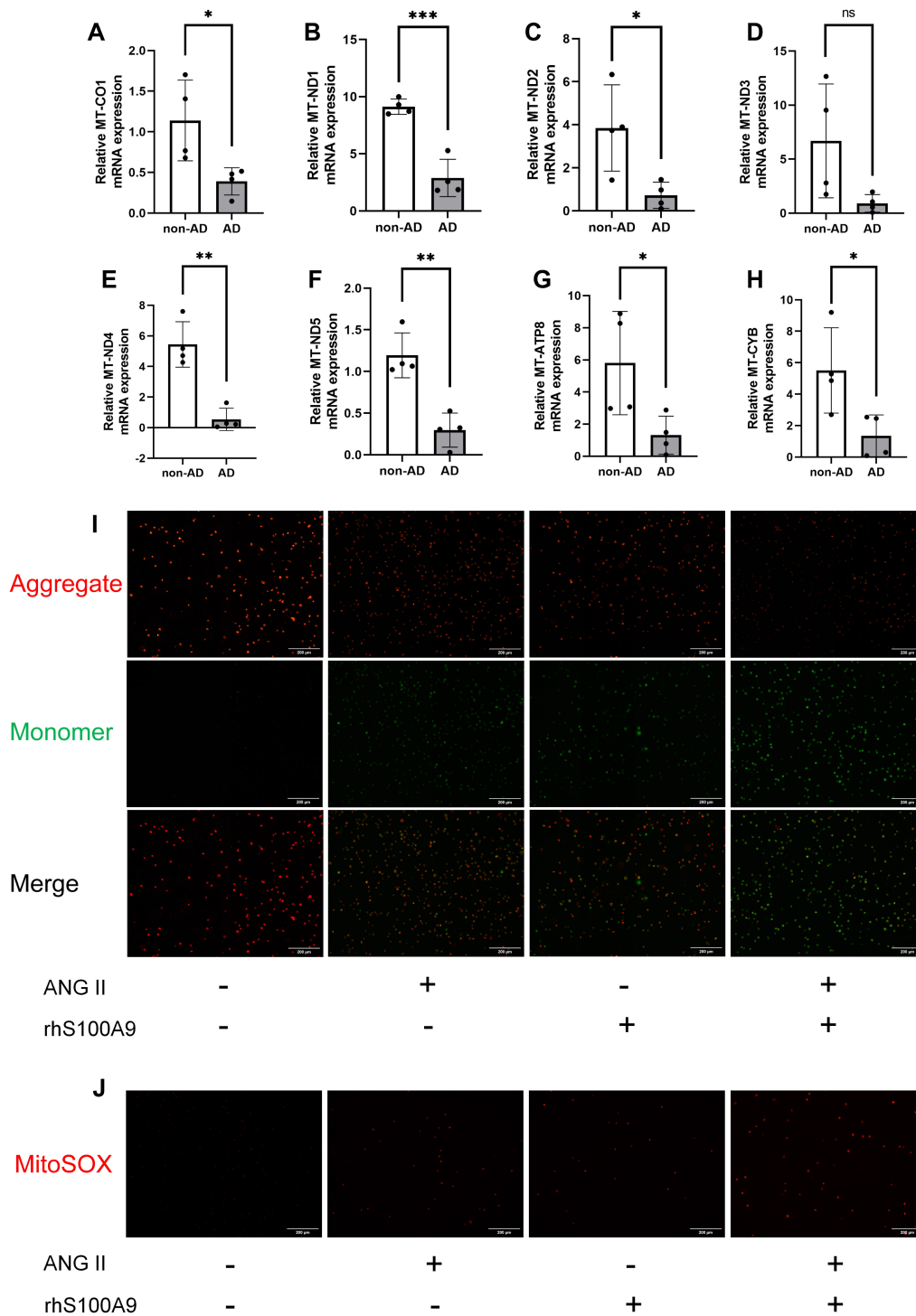


Fig. 6. S100A9 deteriorate mitochondrial quality. (A–H) The core mitochondrial genes mRNA expression in vascular tissues (n = 4). (I) JC-1 fluorescence images of THP-1 cells treated with Ang-II or recombinant human S100A9 (rhS100A9) for 24 hours (scale bar: 200 μ m). (J) MitoSOX fluorescence images of THP-1 cells treated with Ang-II or rhS100A9 for 24 hours (scale bar: 200 μ m). The data are presented as the mean \pm standard error of the mean. ns, no significant difference; * p < 0.05; ** p < 0.01; *** p < 0.001.

tients with type A dissection compared to healthy controls, and that is validated by experiments. This finding aligns with previous research suggesting that S100A9 is involved in inflammatory responses, underscores its relevance in the pathogenesis of aortic dissection [8].

S100A9, a member of the S100 protein family, consists of small calcium-binding proteins that play crucial roles in immune response and inflammation [8]. Some S100A9 inhibitor, such as ABR-215757 and related quinoline-3-carboxamides, have shown promise in preclin-

ical cardiovascular and autoimmune disease models [17]. And another S100A9 inhibitor, Paquinimod, has established safety and pharmacokinetics in early human trials and demonstrates therapeutic efficacy in animal models of fibrosis [18]. Our team also find that S100A9 promotes the progress of sepsis by participating in pulmonary microvascular leakage [10]. S100A9 is often upregulated in response to inflammatory stimuli, participating in the recruitment and activation of immune cells at sites of injury or infection [19]. Elevated levels of S100A9 have been associated with chronic inflammatory diseases, autoimmune disorders, and certain types of cancer [20]. S100A9 also correlates with plaque instability and vascular calcification. Both inflammation, plaque and vascular calcification is known to significantly impact the pathophysiology of aortic dissection through various mechanisms [21]. Thus, we further investigated the effects of S100A9 on aortic dissection using S100A9 KO mice. We observed that S100A9 was markedly increased in the aortic tissues of wild-type mice with induced dissection, while *S100A9* knockout mice showed significantly improved outcomes. The enhanced survival rates and reduced aortic diameter in *S100A9* knockout mice suggest that targeting this protein may offer a promising therapeutic strategy, which is consistent with a recent study using S100A9 inhibitor [11]. This highlights the potential of S100A9 as a therapeutic target for managing aortic dissection.

Our single-cell analysis provided additional insights into the cellular mechanisms by which S100A9 influences aortic dissection. The inhibition of S100A9 altered the composition of cell populations within the aortic tissue, favoring an increase in fibroblasts and smooth muscle cells, which are essential for vascular integrity. Concurrently, there was a reduction in immune and inflammatory cells, indicating that S100A9 plays a role in modulating the inflammatory environment associated with aortic dissection. This shift in cellular dynamics underscores the importance of S100A9 in maintaining vascular homeostasis.

Previous research has indicated that the elevation of nuclear factor kappa B (NF- κ B)-dependent inflammatory responses may contribute to the development of aortic dissection through S100A9 [11]. Inflammation is regulated by various factors, including cytokines and bacterial infections. Recent studies have also shown that mitochondria are involved in regulating immune responses, such as the classical comprised of cyclic GMP-AMP synthase (cGAS), stimulator of interferon genes (cGAS-STING) pathway [22, 23]. Furthermore, improving mitochondrial function has been found beneficial for aortic dissection [24].

Emerging evidence suggests that S100A9 may regulate mitochondrial function indirectly through pattern recognition receptors such as Toll-like receptor 4 (TLR4) and receptor for advanced glycation end products (RAGE) [25,26]. Engagement of these receptors activates NF- κ B and mitogen-activated protein kinase (MAPK) signaling,

which not only drive inflammatory responses but also influence mitochondrial dynamics and oxidative stress [8,27]. S100A9 has also been shown to impair mitochondrial respiration and enhance ROS production, thereby contributing to tissue injury [28]. However, the involvement of mitochondria in the S100A9-mediated pathophysiology of aortic dissection remains unclear. Thus, we further analyzed the single-cell sequence data. Our analysis of single-cell sequencing data revealed significant insights into this area. The observed improvement in mitochondrial quality upon S100A9 inhibition suggests a potential mechanism through which S100A9 contributes to the pathophysiology of aortic dissection. Subsequently, we validated mitochondrial DNA (mtDNA)-encoded gene mRNA expression, the same as our single-cell analysis, revealing significant downregulation in AD patients. Through *in vitro* experiments, we further confirmed that S100A9 impairs mitochondrial membrane potential and increases ROS production in granulocyte. Enhanced mitochondrial function may not only support cellular energy needs but also reduce oxidative stress, which is implicated in vascular damage and inflammation.

Although the protective effects of S100A9 deficiency on AD, therapeutic inhibition of S100A9 should be cautiously considered, as its blockade may induce immunosuppressive effects, given its essential role in innate immunity. Therefore, while targeting S100A9 represents a promising strategy for preventing AD progression, careful evaluation of its safety profile, particularly the risk of immunosuppression, is warranted in future preclinical and clinical studies.

At last, a limitation needs to be pointed out. We used small human cohort size for proteomic analysis, so the future validation in larger, independent patient cohorts would strengthen our results.

5. Conclusions

In conclusion, our study elucidates the critical role of S100A9 in the development of aortic dissection, suggesting S100A9 inhibition may be a novel approach for preventing aortic dissection.

Availability of Data and Materials

All data and methods are available from the corresponding author on a reasonable request.

Author Contributions

KZ and LL interpreted data, prepared the figures and wrote the main manuscript text. KZ and YZ performed the main analysis and LL helped in bioinformatic analysis. KZ and KG performed the animal experiments. ZZ and MW helped with analysis and editing. XW, YZ and YG designed the study, edited the manuscript and earned the funds. XW and YZ were responsible for the clinical samples collection and supervised the project. All authors contributed to editorial changes in the manuscript. All authors read and ap-

proved the final manuscript. All authors have participated sufficiently in the work and agreed to be accountable for all aspects of the work.

Ethics Approval and Consent to Participate

The study involving human samples was conducted in accordance with the principles of the Declaration of Helsinki. Ethical approval was granted by the local ethics committee of the First Affiliated Hospital of Chongqing Medical University (approval number: 2024-173-02). The requirement for informed consent was waived by the committee due to the retrospective nature of the study and the use of anonymized data. All animal experiments were conducted in accordance with the National Institutes of Health Guidelines for the Use of Laboratory Animals and all animal procedures were approved by the Animal Care and Use Committee of Chongqing Medical University (approval number: IACUC-CQMU-2024-04098).

Acknowledgment

Not applicable.

Funding

This work was supported by the Chongqing education committee (KJQN202300480), the doctor “Through Train” project funding of Chongqing Wanzhou district (WZSTC-20220133), Program for Youth Innovation in Future Medicine, Chongqing Medical University (W0168).

Conflict of Interest

The authors declare no conflict of interest.

Declaration of AI and AI-Assisted Technologies in the Writing Process

During the preparation of this work the authors used ChatGpt-4 in order to check spell and grammar. After using this tool, the authors reviewed and edited the content as needed and takes full responsibility for the content of the publication.

Supplementary Material

Supplementary material associated with this article can be found, in the online version, at <https://doi.org/10.31083/FBL44666>.

References

- [1] Yang B, Norton EL, Rosati CM, Wu X, Kim KM, Khaja MS, *et al.* Managing patients with acute type A aortic dissection and mesenteric malperfusion syndrome: A 20-year experience. *The Journal of Thoracic and Cardiovascular Surgery*. 2019; 158: 675–687.e4. <https://doi.org/10.1016/j.jtcvs.2018.11.127>.
- [2] Berretta P, Iafrancesco M, Settepani F, Mele D, Di Giannuario G, Murzi M, *et al.* Follow-up after surgical treatment of type A acute aortic dissection: current evidence and controversies. *Giornale Italiano Di Cardiologia* (2006). 2020; 21: 858–864. <https://doi.org/10.1714/3455.34440>. (In Italian)
- [3] Petrov I, Stankov Z, Vasilev S, Tasheva I, Kozareva G. Endovascular Treatment of Complex Aortic Dissection. A Single Center 5 Years' Experience with 36 Patients. *Reviews in Cardiovascular Medicine*. 2023; 24: 133. <https://doi.org/10.31083/j.rcm2405133>.
- [4] Chen Z, Gao Q, Qiu J, Ge M, Wang S, Liu C, Wu M, He W, Wang J, Chen Y, Zhang H. Genetic analysis reveals Key regulatory Axis in aortic dissection: CBL regulated by HOXB13 and microRNA-1321. *Cardiovascular Innovations and Applications*. 2024; 9: 929.
- [5] Yin ZQ, Han H, Yan X, Zheng QJ. Research Progress on the Pathogenesis of Aortic Dissection. *Current Problems in Cardiology*. 2023; 48: 101249. <https://doi.org/10.1016/j.cpcardiol.2022.101249>.
- [6] Branchetti E, Poggio P, Sainger R, Shang E, Grau JB, Jackson BM, *et al.* Oxidative stress modulates vascular smooth muscle cell phenotype via CTGF in thoracic aortic aneurysm. *Cardiovascular Research*. 2013; 100: 316–324. <https://doi.org/10.1093/cvr/cvt205>.
- [7] Lu HY, Hsu HL, Li CH, Li SJ, Lin SJ, Shih CM, *et al.* Hydrogen Sulfide Attenuates Aortic Remodeling in Aortic Dissection Associating with Moderated Inflammation and Oxidative Stress through a NO-Dependent Pathway. *Antioxidants*. 2021; 10: 682. <https://doi.org/10.3390/antiox10050682>.
- [8] Chen F, He Z, Wang C, Si J, Chen Z, Guo Y. Advances in the study of S100A9 in cardiovascular diseases. *Cell Proliferation*. 2024; 57: e13636. <https://doi.org/10.1111/cpr.13636>.
- [9] Zhao B, Yu J, Luo Y, Xie M, Qu C, Shi Q, *et al.* Deficiency of S100 calcium binding protein A9 attenuates vascular dysfunction in aged mice. *Redox Biology*. 2023; 63: 102721. <https://doi.org/10.1016/j.redox.2023.102721>.
- [10] Yu J, Zhao B, Pi Q, Zhou G, Cheng Z, Qu C, *et al.* Deficiency of S100A8/A9 attenuates pulmonary microvascular leakage in septic mice. *Respiratory Research*. 2023; 24: 288. <https://doi.org/10.1186/s12931-023-02594-0>.
- [11] Jiang H, Zhao Y, Su M, Sun L, Chen M, Zhang Z, *et al.* A proteome-wide screen identifies the calcium binding proteins, S100A8/S100A9, as clinically relevant therapeutic targets in aortic dissection. *Pharmacological Research*. 2024; 199: 107029. <https://doi.org/10.1016/j.phrs.2023.107029>.
- [12] Inciarte-Mundo J, Frade-Sosa B, Sanmartí R. From bench to bedside: Calprotectin (S100A8/S100A9) as a biomarker in rheumatoid arthritis. *Frontiers in Immunology*. 2022; 13: 1001025. <https://doi.org/10.3389/fimmu.2022.1001025>.
- [13] Yu G, Wang LG, Han Y, He QY. clusterProfiler: an R package for comparing biological themes among gene clusters. *Omics*. 2012; 16: 284–287. <https://doi.org/10.1089/omi.2011.0118>.
- [14] Subramanian A, Tamayo P, Mootha VK, Mukherjee S, Ebert BL, Gillette MA, *et al.* Gene set enrichment analysis: a knowledge-based approach for interpreting genome-wide expression profiles. *Proceedings of the National Academy of Sciences of the United States of America*. 2005; 102: 15545–15550. <https://doi.org/10.1073/pnas.0506580102>.
- [15] Yu G. Gene Ontology Semantic Similarity Analysis Using GOSemSim. *Methods in Molecular Biology*. 2020; 2117: 207–215. https://doi.org/10.1007/978-1-0716-0301-7_11.
- [16] Butler A, Hoffman P, Smibert P, Papalexi E, Satija R. Integrating single-cell transcriptomic data across different conditions, technologies, and species. *Nature Biotechnology*. 2018; 36: 411–420. <https://doi.org/10.1038/nbt.4096>.
- [17] Schiopu A, Cotoi OS. S100A8 and S100A9: DAMPs at the crossroads between innate immunity, traditional risk factors, and cardiovascular disease. *Mediators of Inflammation*. 2013; 2013: 828354. <https://doi.org/10.1155/2013/828354>.
- [18] Miura S, Iwamoto H, Namba M, Yamaguchi K, Sakamoto S, Horimasu Y, *et al.* High S100A9 level predicts poor sur-

- vival, and the S100A9 inhibitor paquinimod is a candidate for treating idiopathic pulmonary fibrosis. *BMJ Open Respiratory Research*. 2024; 11: e001803. <https://doi.org/10.1136/bmjresp-2023-001803>.
- [19] Xia P, Ji X, Yan L, Lian S, Chen Z, Luo Y. Roles of S100A8, S100A9 and S100A12 in infection, inflammation and immunity. *Immunology*. 2024; 171: 365–376. <https://doi.org/10.1111/imn.13722>.
- [20] Wang S, Song R, Wang Z, Jing Z, Wang S, Ma J. S100A8/A9 in Inflammation. *Frontiers in Immunology*. 2018; 9: 1298. <https://doi.org/10.3389/fimmu.2018.01298>.
- [21] Averill MM, Kerkhoff C, Bornfeldt KE. S100A8 and S100A9 in cardiovascular biology and disease. *Arteriosclerosis, Thrombosis, and Vascular Biology*. 2012; 32: 223–229. <https://doi.org/10.1161/ATVBAHA.111.236927>.
- [22] Guo Y, You Y, Shang FF, Wang X, Huang B, Zhao B, *et al*. iNOS aggravates pressure overload-induced cardiac dysfunction via activation of the cytosolic-mtDNA-mediated cGAS-STING pathway. *Theranostics*. 2023; 13: 4229–4246. <https://doi.org/10.7150/thno.84049>.
- [23] Zhou G, Wang X, Guo M, Qu C, Gao L, Yu J, *et al*. Mitophagy deficiency activates stimulator of interferon genes activation and aggravates pathogenetic cardiac remodeling. *Genes & Diseases*. 2024; 11: 101074. <https://doi.org/10.1016/j.gendis.2023.08.003>.
- [24] Sun T, Yuan W, Wei Y, Liao D, Tuo Q. The Regulatory Role and Mechanism of Energy Metabolism in Vascular Diseases. *Frontiers in Bioscience (Landmark Edition)*. 2024; 29: 26. <https://doi.org/10.31083/j.fbl2901026>.
- [25] Li J, Hu R, Liu X, Peng L, Yi J, Zhong X, *et al*. S100A9/RAGE pathway regulation of mitophagy and the effect of JianPi LiShi YangGan formula in acute-on-chronic liver failure. *Journal of Ethnopharmacology*. 2025; 348: 119887. <https://doi.org/10.1016/j.jep.2025.119887>.
- [26] Shi W, Wan TT, Li HH, Guo SB. Blockage of S100A8/A9 ameliorates septic nephropathy in mice. *Frontiers in Pharmacology*. 2023; 14: 1172356. <https://doi.org/10.3389/fphar.2023.1172356>.
- [27] Xu Y, Wang Y, Ning K, Bao Y. Unraveling the Mechanisms of S100A8/A9 in Myocardial Injury and Dysfunction. *Current Issues in Molecular Biology*. 2024; 46: 9707–9720. <https://doi.org/10.3390/cimb46090577>.
- [28] Huo S, Wang M, Du M, Ren B, Yang T, Peng L, *et al*. Macrophage-derived S100A9 promotes diabetic cardiomyopathy by disturbing mitochondrial quality control via STAT3 activation. *International Journal of Biological Sciences*. 2025; 21: 3061–3080. <https://doi.org/10.7150/ijbs.111128>.